Wideband Gyro-Amplifiers

C. G. Whyte, K. Ronald, A. R. Young, W. He, C. W. Robertson, D. H. Rowlands, and A. W. Cross

***Abstract*—Gyro-amplifiers using helically corrugated waveguides have shown exceptional gain, power, bandwidth, and efficiency performance at cm and mm wavelengths. The performance of a long pulse (and therefore high vacuum) system is strongly influenced by factors other than the intrinsic bandwidth of the interaction. We shall discuss these and other challenges, along with their mitigation in high average power wideband amplifiers.**

***Index Terms*—Electron tubes, gyrotrons, microwave amplifiers, microwave devices.**

I. Introduction

BROADBAND MICROWAVE amplifiers have significant advantages over oscillators of similar output power for a number of applications. For instance, in spherical tokomaks, electron Bernstein waves can be used to investigate transport and stability phenomena [1] as well as provide plasma heating and current drive [2]. These applications can occur over a range of frequencies, and a tunable source would have significant advantages. Experimental and theoretical investigations of wideband amplifiers at MW power levels in the centimeter to millimeter wavelength range have shown that devices with greater than 20% bandwidth, suitable for long pulse to CW operation, are a practical proposition. This paper is organized as follows: in Section II, we discuss the theory of gyro travelling wave amplifiers, in Section III, magnetic cusp electron guns are discussed. Section IV explores the issues surrounding amplifier stability, while Section V addresses broadband component design. Conclusions are given in Section VI.

II. Amplifier Theory

The gyro-TWT [3] is an amplifier variant of the broad class of gyro-devices where electrons move along helical trajectories inside a waveguide, immersed in a uniform magnetic field $\vec{B}_0 = B_0\vec{z}_0$. The electron cyclotron frequency, $\omega_H = eB_0/\gamma m_0$, depends on the electron energy via the relativistic factor γ of the electrons. Electrons whose energy has been modified by interaction with a wave will rotate with a range of frequencies and so gather into azimuthal bunches. With correct phasing of the bunches, the wave may be either amplified or attenuated. An important advantage of the gyro-TWT is its ability to amplify waves propagating in smooth waveguides, i.e., fast waves [4] not localized near a microwave structure. This feature allows operation at shorter wavelengths and higher power levels than conventional TWTs.

Conventional gyro-TWTs use a smooth cylindrical metal waveguide; this leads to a number of problems. Broadband operation demands operation at grazing incidence where the beam dispersion overlaps with the wave and the axial electron velocity is close to the group velocity of the wave. The intersection occurs close to cutoff for subrelativistic electrons, and low-frequency gyrotron oscillation is not easily suppressed. If low-frequency oscillation can be controlled, Doppler broadening of the cyclotron resonance line and the spread in the axial electron velocity combine to decrease the efficiency at the upper edge of the frequency band. For these reasons, subrelativistic gyro-TWTs have significantly lower efficiency than gyrotrons.

In the relativistic case, axial wavenumbers are even larger. The Doppler frequency shift is very important; this regime is attractive for high-frequency radiation production, but like cyclotron auto-resonance masers, and, unlike the gyrotron, it is very sensitive to the spread in electron velocity.

Many techniques have been applied to "conventional" gyro-TWTs to improve their performance, including profiling the magnetic field and the waveguide cross section [5]–[7] and applying distributed losses [8]–[10].

The ideal dispersion for a broadband gyro-TWT waveguide has a constant wave group velocity with significant gradient in the region of low axial wavenumbers. Such a dispersion may be conveniently matched to the electron axial velocity in the region of low wavenumbers, the gradient giving rise to an extended frequency range. As shown in [11]–[13], the necessary dispersion may be realized, over a broad frequency band, in an oversized circular cylindrical waveguide with a helical corrugation of the inner surface:

$$r(\varphi, z) = r_0 + l\cos(m\bar{}\varphi + h\bar{}z) \tag{1}$$

where r, φ, z are cylindrical co-ordinates, r_0 is the waveguide mean radius, l, $\bar{m}$, and $\bar{h} = 2\pi/d$ are the amplitude, azimuthal, and axial numbers of the corrugation, respectively, and d is the corrugation period. The corrugation couples two partial rotating waves of a waveguide with a radius of r_0; one partial wave is near-cutoff, mode (A), and has a small axial wavenumber, $h_A \ll k$, where $k = \omega/c$, while the other partial wave, a traveling wave (B), has a large axial wavenumber, $h_B \sim k$. The axial wavenumbers and azimuthal indices of the waves and the corrugation should satisfy the Bragg conditions

$$h_B \approx \bar{h}, \quad m_A + m_B = \bar{m}. \tag{2}$$

Manuscript received October 3, 2011; revised February 11, 2012; accepted February 28, 2012. Date of publication April 13, 2012; date of current version May 9, 2012. This work was supported in part by the EPSRC, STFC and DSTL.

C. G. Whyte, K. Ronald, A. R. Young, W. He, C. W. Robertson, and A. W. Cross are with the The Physics Department, The University of Strathclyde, G4 0NG Glasgow, U.K. (e-mail: colin.whyte@strath.ac.uk; kevin.ronald@strath.ac.uk; a.r.youg@strath.ac.uk; w.he@strath.ac.uk; c.w.robertson@strath.ac.uk; a.w.cross@strath.ac.uk).

D. H. Rowlands was with the The Physics Department, The University of Strathclyde, G4 0NG Glasgow, U.K.. He is now with e2v Technologies Ltd, CM1 2QU Chelmsford Essex, U.K. (e-mail: david.rowlands@starth.ac.uk).

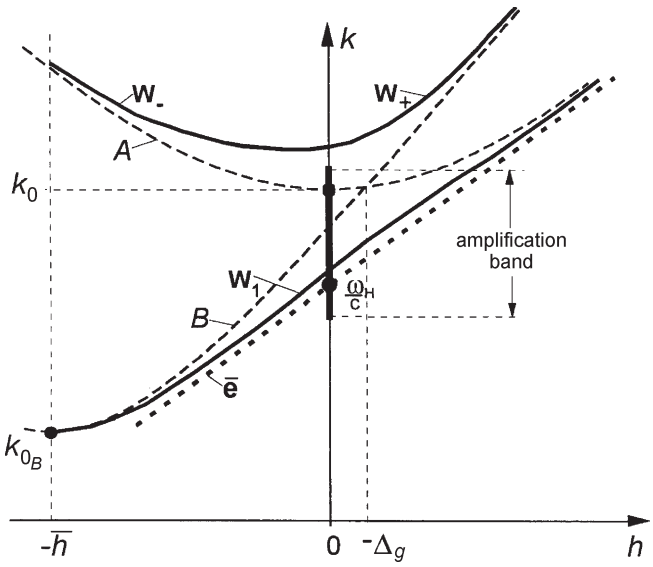

Fig. 1. Dispersion diagram for a helical waveguide: A, B—the partial near-cutoff and traveling waves of a smooth waveguide, respectively, which are coupled due to the helical corrugation of the inner surface, W1 and W±—the operating and "spurious" eigenwaves of the helical gyro-TWT, $\bar{e}$—unperturbed electron cyclotron wave.

The resonant coupling of the waves occurs at the intersection between the mode A and the first spatial harmonic of the wave B with cutoff frequencies ω_0 and ω_{0B}, respectively (Fig. 1).

If the corrugation amplitude l is small compared with the wavelength, the method of perturbation can be used with reasonable accuracy to calculate the dispersion characteristics of the helical waveguide [11]–[13]. The resultant eigenwaves, which arise as a result of coupling the partial waves A and B, can then be found. When the parameters of the corrugation are properly chosen, the wave W_1 has the desirable dispersion.

The frequency gap between W_1 and "spurious" waves $W_\pm$ in the region of "zero" axial wavenumbers is of the order of the coupling coefficient of the waves σ, which is proportional to the relative amplitude of the corrugation l/r_0 and depends also on the azimuthal and radial indices of the partial waves. For a relatively small corrugation depth, when $\sigma \leq 0.1$, the method of perturbation provides good agreement with "cold" experiments.

If the amplification parameter C is much smaller than the coupling coefficient σ, the electron beam does not significantly change the dispersion characteristics, and the electrons can be coupled with the cold eigenwave W_1 as shown in Fig. 1. The attractive dispersion relation as represented in Fig. 1 can be obtained by tuning the magnetic field for synchronism $\omega_1 - h_1 v_\parallel \approx s\omega_H$ (here s is the cyclotron harmonic number) between the desirable wave with frequency ω_1 and axial number h_1 and the electrons moving with axial velocity $v_\parallel$. For this situation, the fifth-order dispersion equation of a helical gyro-TWT can be reduced to a third-order equation

$$(h-h_1)\left[h-\frac{(\delta-\Delta_{\rm H})}{\beta_{\parallel_0}}\right]^2=\hat{C}^3\left\{1+\left(\frac{2s\beta_{\parallel_0}}{\beta^2_{\perp_0}}\right)\left[h-\frac{(\delta-\Delta_{\rm H})}{\beta_{\parallel_0}}\right]\right\} \quad (3)$$

which is identical to that for a conventional gyro-TWT with a smooth waveguide. h and h_1 have been normalized to $k_0 = \omega_0/c$. $\delta = (\omega - \omega_0)/\omega_0$ and $\Delta_H = (s\omega_H - \omega_0)/\omega_0$ are the normalized frequency and magnetic field mismatches, respectively, $\beta_{\parallel_0} = v_{\parallel_0}/c$ and $\beta_{\perp_0} = v_{\perp_0}/c$ are the normalized axial and transverse electron velocities, respectively, and $\hat{C} = C(\chi/2)^{1/3}$ is the modified amplification parameter of the wave. The coefficient $\chi = 2(h_1 + \Delta_g - \delta/h_0)/[3h_1^2 + 2h_1(\Delta_g - \delta/h_0) - 2\delta]$ is responsible for the content of the resonant partial mode A in the operating eigenwave W_1, where $\Delta_g = \bar{h} - h_0$ and $h_0 = |h_B(\omega_0)|$ are also renormalized to k_0. In (3),h_1 is a function of δ and describes the "cold" dispersion of the operating eigenwave of the helical waveguide. For the usual gyro-TWT, $\chi = 1/\beta_{gr}$, where β_{gr} is the normalized group velocity in a smooth waveguide.

The analysis of (3) shows that for a large region of electron parameters, including subrelativistic and relativistic energies, a very broad frequency-band gain can be obtained by optimizing the parameters of the corrugation and the value of the magnetic field. A good agreement between solutions of the simplified (3) and a more exact fifth-order equation up to $\sigma \sim C$ demonstrates the correctness of the approach of the dominant interaction of electrons with the eigenwave of the "cold" system. This approach allows a similar simplification of the nonlinear analysis which can be performed using the equations of the usual gyro-TWT with changed dispersion $h_1(\omega)$ and coefficient χ.

Inspection of the helical gyro-TWT dispersion curves (Fig. 1) indicates that mode $W_\pm$ can be easily excited like the operating mode of a conventional gyrotron oscillator due to the region with small group velocity. However, the magnetic field required for excitation of the $W_\pm$ mode is significantly higher than the operating regime because of the separation between curves W_1 and $W_\pm$.

This waveguide was found to be a significant improvement over the conventional smooth cylindrical waveguide in gyro-amplifier systems by decreasing the sensitivity to electron velocity spread, increasing the stability to parasitic self-oscillations, and improving the frequency bandwidth. Due to these properties, such waveguides [14] have been used in a wide range of applications, e.g., interaction regions in gyro-amplifiers and gyro-BWOs [15] as well as in passive pulse compressors [16] capable of GW level powers at X-band. Gyro-amplifiers using helically corrugated waveguides have shown exceptional gain, power, bandwidth, and efficiency performance at cm and mm wavelengths. Hereafter, the nomenclature Gyro-TWA is adopted to denote a gyro-amplifier using a helically corrugated waveguide while gyro-TWT is used to refer to a smooth bored device.

III. Magnetic Cusp Electron Gun

Gyro-devices such as the gyro-TWA which operate at a harmonic of the electron cyclotron frequency (harmonic number $s > 1$) have a reduced magnetic field requirement for a given frequency of operation. Operation with a high-order waveguide mode (TE_{mn}, where m or n are > 1, m, n are, respectively, the azimuthal and radial mode indices) is also attractive to maximize the cavity size and power handling capability. In so doing, it becomes attractive to use an axis-encircling (large orbit) electron beam to mitigate the problems of parasitic

oscillation. A large orbit beam of this form can excite only resonant modes with azimuthal indices equal to the cyclotron harmonic number $s = m$.

Axis encircling beams can be conveniently generated using a Pierce type electron gun to generate a conventional solid electron beam on axis; a "kicker coil" or "wiggler" is then used to impart transverse momentum to the electron beam and produce a "solid" helically propagating axis-encircling electron beam. Space charge forces then cause the "corkscrew" type beam to spread in Θ to produce a cylindrical beam of electrons with axis encircling trajectories. The kicker magnets used may be electrically driven or constructed from permanent magnets or a combination of the two techniques. Electromagnetic kickers have the advantage of adjustability which can be an important consideration.

A more attractive way to impart transverse velocity to the electrons in the beam arose from the study of charged particle motion under nonadiabatic reversal of the magnetic field. This so-called "cusp" method [17], which was initially researched for applications in plasma confinement, could produce an annular, axis-encircling electron beam with the high pitch factor (ratio between transverse velocity and axial velocity) required for gyro-devices. This has inherent advantages over a "solid" electron beam. Energy recovery is easier due to the reduced beam power density on the collector surface. CW or long pulse amplifiers are often limited by their "kicker coil" which have limited duty. If the need for a kicker coil is removed, one factor limiting performance need no longer be considered.

Most studies of electron beam dynamics have been based on the configuration where the magnetic cusp was located at or near the anode. These designs require sharp changes in a high magnitude axial magnetic field over short distances, often requiring the use of multiple coils or high μ materials in the gun region.

If, instead, the sharp cusp is placed close to the cathode, considerable simplification of the magnetic system is possible, a "smooth" cusp formed by two coils with no magnetic shaping pole pieces can be used to generate the required axis-encircling electron beam.

Where both the magnetic and electric fields are azimuthally symmetric, conservation of the electron canonical angular momentum gives rise to (4). The right-hand side of (4) describes the electrons' motion at the initial position near the cathode, while the left-hand side describes their motion at their final position, immersed in a uniform magnetic field:

$$m_0\gamma r_0^2\dot{\theta} - er_0^2B_0/2 = er_c^2B_c/2 \tag{4}$$

where B is the magnetic field, γ is the relativistic factor of the electron beam, e and m_0 are the electric charge and rest mass of an electron, r and Θ are the radial and azimuthal co-ordinates and $\dot{\theta}$ denotes the derivative of Θ with time. Subscripts "0" and "c" denote the final and cathode region, respectively.

For an axis-circling beam where

$$\omega_0 = \dot{\theta} = \frac{eB_0}{\gamma m_0} = \frac{V_\perp}{r_0}$$

it is possible to show that:

$$\alpha = \frac{V_\perp}{V_z} = \sqrt{\frac{-r_c^2\omega_c\omega_0}{V^2 + r_c^2\omega_c\omega_0}}$$

$$r_c = r_0\sqrt{\frac{-B_0}{B_c}}. \tag{5}$$

Here, V and ω are the electron velocity and the cyclotron frequency, subscript "$\perp$" and "z" denote the transverse and z components.

If the magnetic cusp is placed near the cathode two benefits accrue. First, as $B_c \ll B_0$, the magnitude of the required magnetic field reversal is reduced. Second, as the condition for nonadiabaticity is related to the Larmor step L and $L \approx 2\pi V_z/\omega_c$ is inversely proportional to the transverse velocity, the field reversal must occur over a much larger axial distance then would be the case when the cusp is near the anode. In the cathode region, L is estimated to be of the order of meters for a mildly relativistic electron and a cusp amplitude of a few tens of Gauss, much larger than the cusp dimension of a few millimeters satisfying the nonadiabatic condition.

Using (4) and substituting values of V, α and B_0 determined by consideration of the required parameters of the electron beam, it is possible to calculate $r_c^2B_c$.

From (5), the smaller cusp magnitude implies a greater cathode radius. For a given allowed cathode current density, this allows a smaller cathode radial width which in turn reduces the spread in α in the final beam (α is proportional to Δr_c from (5).). The factor limiting the maximum cathode radius is the minimum allowable magnetic field on the cathode. This parameter must be maintained above the level where stray magnetic fields (and ultimately the earth's magnetic fields) can influence operation of the electron gun. Cathode heater coils, etc., must be designed with this in mind. Numerical confirmation by simulation [18] using the 3-D PIC code MAGIC [19] and experimental validation of a "smooth" cusp gun are presented in [17].

The parameters of the electron beam were: beam energy $E = 130$ keV, current $\sim$40 A with $\alpha = 1$ and $B_0 = 0.21$ T. These parameters were chosen for a high-power helical waveguide based gyro-TWA experiment designed for accelerator applications with the intention to extend this design to long pulse operation with a thermionic cathode. The results of the amplifier experiment are currently in preparation. In the long pulse (and therefore high vacuum) case considered here, the system performance is strongly influenced by factors other than the intrinsic bandwidth of the interaction.

IV. Amplifier Stability

Broadband amplifiers present an additional challenge in assuring stability over the full range of frequencies where significant gain is present. If the amplifier round trip gain exceeds the round trip losses, oscillation will occur, and frequency, amplitude and phase control will be lost. This is the main criterion determining the required performance of the components in the gain path and should be considered before a meaningful

specification of those components can be determined. Both the Raman FEL and the gyro-TWA have polarization-dependent gain; that is, gain is experienced only by a wave travelling in the correct direction with the correct polarization. This is particularly important in considering the round trip losses, as, in each case, the losses are strongly influenced by the polarization. When a circularly polarized wave reflects, its polarization changes from left to right or vice versa.

Consider a simplified amplifier consisting of only those components essential to operation, input coupler, gain medium, and output window. We assume the input coupler couples to only one of the two possible linear polarizations of the circular waveguide. We can represent the input signal as two counter propagating circularly polarized waves of equal amplitude. Only one of these circularly polarized waves experiences gain, the input signal can therefore be considered to have experienced a loss of 3 dB. The signal is then amplified, and a proportion is reflected from the output window. This reflection has opposite polarization and returns to the input coupler where it experiences a 3-dB loss. (A circular polarized wave can be represented as two plane polarized waves of equal amplitude with a 90° phase shift, one of which is coupled out of the input coupler, the other is reflected with near 0-dB loss.) The round trip loss is therefore equal to the window return loss plus 6 dB.

In the case where a waveguide polarization converter is included between the input coupler and the gain medium, a different set of circumstances arise. In this case, the linear input wave is converted into circular polarization with high efficiency. Gain and reflection occur as before, but in returning through the polarization converter in the reverse direction, the wave is converted into a wave with linear polarization orthogonal to the input signal. This wave reflects with high efficiency from the input coupler, but on traversing the polarization coupler for a third time emerges with a circular polarization of the opposite hand and so experiences no gain. A further round trip is therefore required before the wave experiences gain once more. This leads to a much improved stability margin for amplifiers with this characteristic as the round trip loss includes double the window return loss and the input coupler return loss for correctly polarized radiation. In practice, this leads to stable gain figures twice as high (46 dB versus 23 dB) as experienced in amplifiers where the stability criterion is for a single pass. It should be noted that this stability criterion can easily be lost, if additional polarization converting components are introduced or their position altered within the amplifier. For instance, if linear output polarization is required, one might consider the addition of another converter within the vacuum envelope, before the output window. This addition returns the amplifier stability calculation to that of the single pass configuration for all reflections which occur after the second polarization converter. Reflections which originate before the second polarization converter are unaffected. Unfortunately, in most cases, the most problematic reflection comes from the output window or other downstream components. An additional complication arises because the output window is often oversized in order to allow the propagation of high power radiation without breakdown. This largely precludes the positioning of a second waveguide type polarization converter after the output window, because the required down taper would have reflection performance which would outweigh any possible advantage. Subsequent polarization control must be achieved by other means.

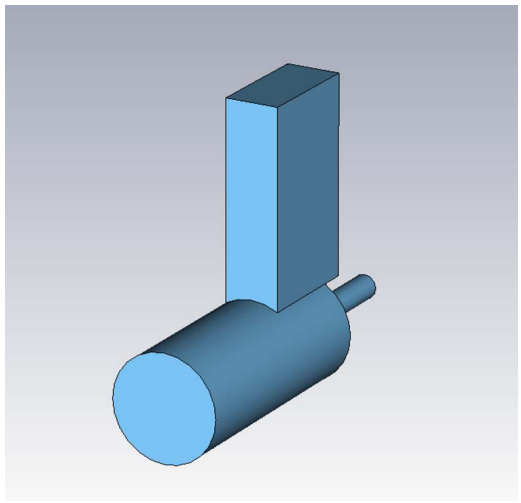

Fig. 2. Input coupler showing rectangular input arm, small diameter electron beam port, and circular port leading to interaction region.

V. Broadband Component Design

A. Input Coupler

All amplifiers require an input port through which the initial signal can be coupled to the interaction region. Typically, this will be a waveguide structure with three ports: the radiation input port, a port through which the incoming electron beam propagates, and a third port where the radiation and electron beam copropagate. We require that the input radiation does not propagate back through the electron beam input port as this may lead to any of a number of problems associated with radiation in the electron gun. An input coupler with a 20% bandwidth around the center frequency can be conveniently designed in conventional rectangular and circular waveguide. Because the frequency range is limited, the output waveguide diameter can be chosen such that the TE_{21} mode is cut off at all frequencies of interest. As the coupler can be configured such that minimal coupling to the TM modes occurs, the output can be restricted to the TE_{11} mode of the circular waveguide. The electron beam port can be sized such that it is significantly below cut off for all frequencies in the range provided an electron beam with low transverse velocity is used in the input coupler region. (The transverse electron velocity component required in the interaction region can be introduced downstream of the input coupler.) See Fig. 2.

The simple input coupler configuration shown in Fig. 2 can be substantially improved by the addition of impedance matching steps in the rectangular to circular transition. Significant improvements to the amplifier stability margin can be gained by the implementation of these techniques.

In the case where a cusp electron gun is used, axis encircling electron trajectories are generated in the electron gun region in contrast to the case of a conventional Pierce-type electron gun where electron trajectories are largely axial and close to the

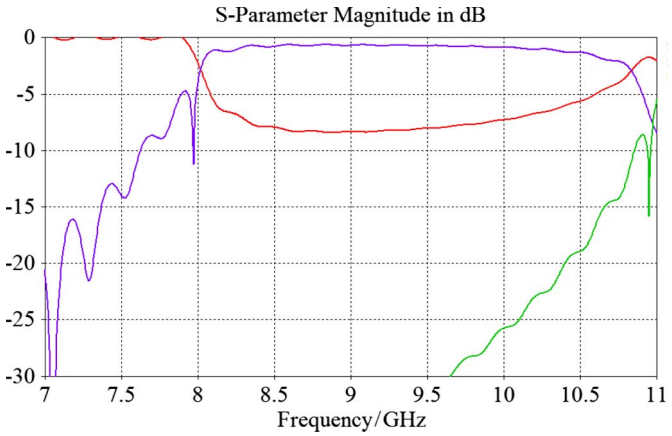

Fig. 3. Input coupler $^{--}S_{11}$, $^{--}S_{21}$, $^{--}S_{31}$ parameters for an increased diameter beam port for use with magnetic cusp electron gun, where port 1 is the rectangular waveguide port, port 2 is the larger circular port and port 3 is the smaller diameter electron beam port.

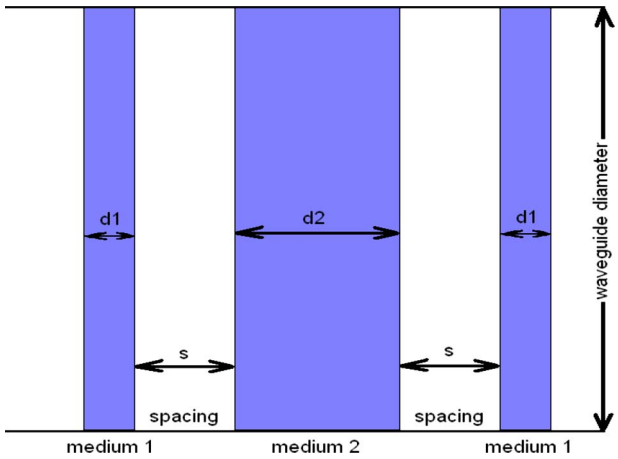

Fig. 4. Five-layer window schematic.

beam axis. As the electron gyro-radius is large compared to the beam diameter, the envelope of the electron beam in the region of the input coupler can be multiplied by up to a factor of four. The electron beam port is then only slightly below cut off for the higher frequencies, and coupler efficiency is compromised. In this case, an alternate form of reflector may be required. If the application can be adequately served by a reduced bandwidth source, a resonant cavity may be used as a reflector. In this case, the amplifier waveguide must be modified to reduce the bandwidth of amplification, otherwise, oscillation outside the band of the input coupler is highly likely. When 20% bandwidth is required, the input coupler return loss may be degraded by over 10 dB in comparison to the optimized case for a pierce type electron gun. Such a reduction in performance does not usually present a problem in terms of amplifier efficiency as the majority of the input signal is still coupled to the interaction region, but the amplifier stability margin will be reduced. The s-parameters for an input coupler suitable for use with a cusp electron gun are shown in Fig. 3.

B. Output Window

The output window of a broadband fast wave amplifier is often the limiting factor in determining the maximum stable gain of the amplifier. The design of narrow band high power windows at high frequencies is well advanced with high quality CVD diamond free space windows propagating 1 MW continuously for 30 min at 170 GHz [20]. This is made possible by the use of resonant window structures. Such an approach cannot operate over a broad frequency band, and some form of matching structure is required. A number of approaches have been tried including double disc windows, Brewster angle windows for linear polarization, low dielectric constant materials such as boron nitride and five-layer windows. Of these techniques, five-layer windows offer the highest bandwidth for circularly polarized radiation.

These windows use three separate dielectric elements separated by vacuum or air spaces to achieve reduced reflection over a broad frequency band. This is achieved by generating additional resonant pass bands on the higher and lower frequency sides of the pass band that would be generated by a single dielectric element. The combined effect of the three pass bands is a broadened transmission window where ultimate transparency is traded for increased transmission at the band edges.

Conventional modeling of multilayer windows using commercial codes, such as Microwave Studio (MS) can be successful, but time consuming. This makes these codes unattractive to use in the design phase as the time per iteration is excessive and optimization of the design is limited by the time available. In highly overmoded structures such as high power windows, the simulation time can easily exceed 24 h and require a fast machine with considerable memory.

The design of a five-layer window (so called because there are five axial dimensions to optimize) is complicated by the large number of independent variables. We have developed a code using the scattering matrix formulation to calculate the transmission, return, and dissipation characteristics of a multilayer window, including waveguide effects [5]. This code does not allow the introduction of angular offsets, azimuthal asymmetry, radial variation or any type of nonuniformity, as can be performed in MS, but it does complete the calculation in less than a second on an average desktop PC.

This speed of calculation allows the use of a simple routine to explore a parameter space described by the designer to determine the optimum window design for maximum return loss. A “brute force” approach can be used evaluating all possible combinations with a given parameter space, subject to manufacturing constraints. Our routine is further accelerated by choosing a reference desired return loss figure, with this target specification, the routine is configured to cease further calculation on any geometry the moment a return figure poorer than the target value is returned. As the routine calculates 1000 points for each geometry, this can result in a substantial time saving. It is also possible to reconfigure the routine to, for instance, minimize the power dissipation in the window which may be desirable when the transmitted power is particularly high.

A five-layer window design (Fig. 4, side layer-air gap-main window-air gap-side layer) can typically be optimized in less

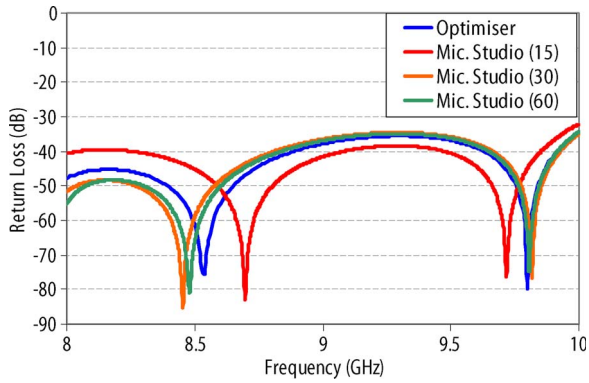

Fig. 5. Comparison of MS and scattering code.

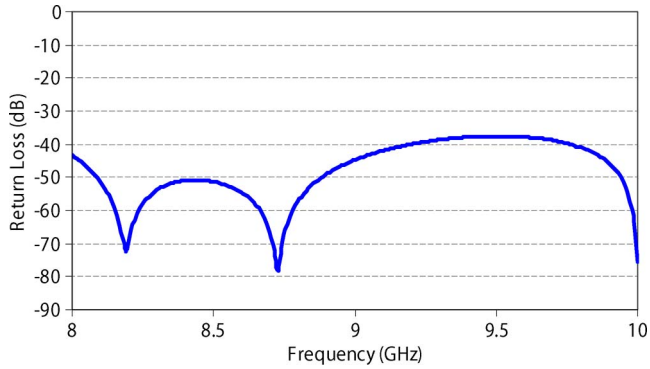

Fig. 6. Optimized five-layer window design.

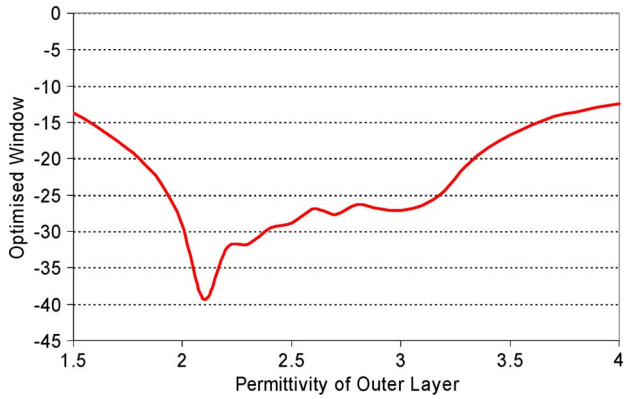

Fig. 7. Return loss as a function of refractive index for three-layer window.

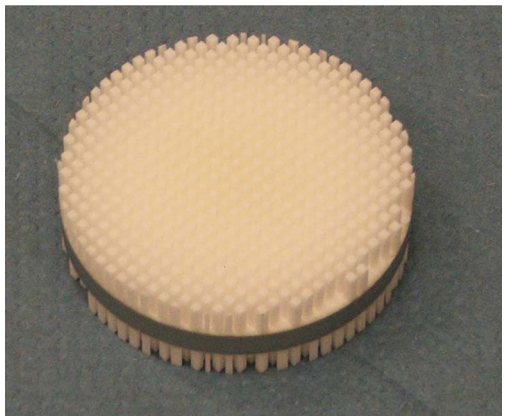

Fig. 8. Machined ceramic window.

than 1 h to dimensional tolerances of 0.1 mm. Tolerance analysis can be included to ensure that the calculated geometry performance does not degrade significantly when errors within the manufacturing tolerances are included.

The scattering matrix formulation output was compared to that from MS, when a range of numbers of mesh cells per wavelength were used in MS (see Fig. 5). From this result, we can see that the agreement between the codes improved as the number of mesh cells was increased. While this is not an indication of which code will agree with measurement, one would expect MS accuracy to improve with increased number of mesh cells. The 60 cells per wavelength simulation took almost a week on a fast, multiprocessor machine with 16 GB of RAM.

An earlier window designed using Comsol MultiPhysics was used as the starting point of our design process. This window was not a UHV compatible design and used quartz as the window material. This design was modeled in MS and with the new scattering matrix code to benchmark the new code. The design was then changed to use alumina as the central window disc, to allow this layer to form the UHV-compatible vacuum seal. Quartz was retained for use in the side windows as the high refractive index of alumina would result in rather thin components were it to be used. The routine was then run with a 0.1 mm step size and a 0.5 mm minimum window thickness; the results are shown in Fig. 6.

The new design has a minimum return loss in the frequency range of interest of approximately 37 dB as compared to 24 dB for the original design.

This design can be repeated for all alumina designs or indeed any material of choice.

Scattering matrix methods cannot account for angular misalignment, this requires full 3-D simulation. The scattering matrix method is, however, excellent for assessing sensitivity to tolerances.

Five-layer windows offer excellent performance but require accurate manufacture. In practice, manufacturing tolerances for the thickness of the dielectric elements are achieved trivially. Accurate alignment of the discs relative to each other is the deciding factor determining performance. If we move instead to a three-layer design, where layers of lower refractive index are placed in contact with the central disc, manufacturing accuracy is much improved. The design of such a window is facilitated by the use of a mdified scattering matrix routine. The refractive index is now introduced as a variable and as there are now only three axial dimensions available; the optimal window respsonse as a function of permittivity for the three-layer window can be calculated, see Fig. 7.

Materials of arbitrary permittivity are generally not available; one way to tailor the dielectric permittivity is to “machine” a “city block” structure into each of the two flat faces of a ceramic disc. See Figs. 8 and 9.

If the material removal is performed on a scale smaller than the wavelength of the radiation transmitted (wavelength in the dielectric, not wavelength in free space), the propagating wave is subject to an effective permittivity which may be derived from analytic theory. The effective permittivity is a

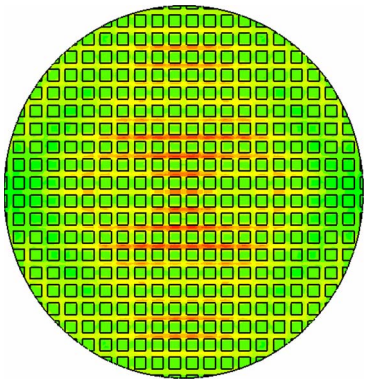

Fig. 9. Microwave Studio model of machined ceramic window.

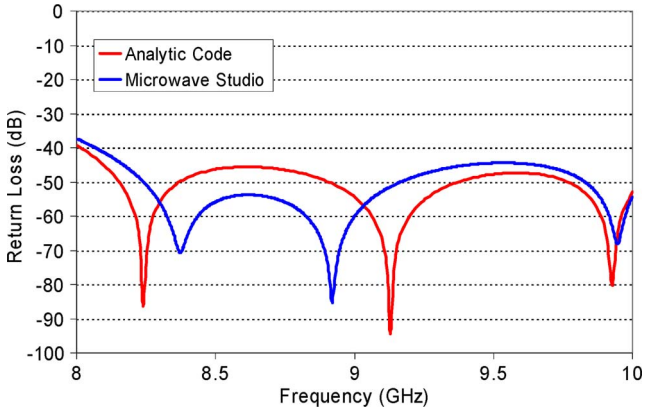

Fig. 10. Return loss as a function of frequency for machined ceramic three-layer window.

relatively strong function of fill factor, and machining accuracy is important.

The permittivity may also be simulated in MS, by calculating the phase shift associated with a section of material. This calculation is numerically intensive as the structure is heavily overmoded and loaded with material of relatively high permittivity. The model requires a large number of cells, and simulations are time consuming.

If the desired effective permittivity can be produced, simulations show that good window performance can be achieved.

The window shown in Figs. 8 and 9 was manufactured for use in x-band, machined from high purity alumina. The design parameters were: side dielectric thickness 6 mm, 1 mm wide "streets" on a 3 mm pitch to give an effective permittivity of 2.1. The central disc was 5 mm thick. Overall, ceramic diameter was 60 mm. The calculated response of this window is shown in Fig. 10.

The manufactured component failed to meet the specified geometric tolerances. The side dielectric's thickness was reduced from 6 mm to 5.75 mm, while the effective fill factor was reduced from 0.38 to 0.34. This resulted in a decrease in effective relative permittivity from 2.1 to 1.9. Simulations showed the measured performance agreed well with simulations of the design when the "as manufactured" parameters were used, see Fig. 11. In Fig. 11, the continuous curve represents simulated results, while the two remaining lines show results for measurements made in the two waveguide bands of interest.

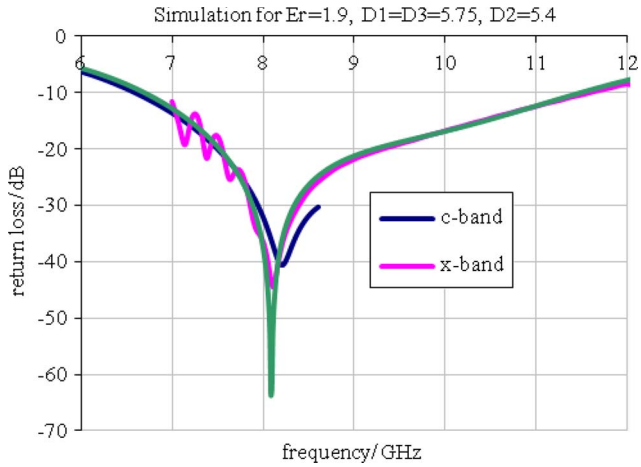

Fig. 11. Measured return loss as a function of frequency for machined ceramic window.

Windows with bandwidths significantly exceeding 20% of center frequency cannot be designed with discrete elements, and an alternative approach must be taken. In devices where a low vacuum environment is acceptable, thin Mylar windows can be used to great effect. 60 mm diameter windows of 0.1 mm thick Mylar have excellent return loss figures at cm wavelengths. Replicating this performance in a high vacuum system can be approached with thin diamond windows grown in a "dome" shape to enhance the physical strength of the diamond. Diamond is an excellent low loss dielectric in the cm to mm wavelength range with high thermal conductivity, high stiffness, and high stress before failure. Diamond can be brazed to UHV standard. Industrial diamond is cost effective, and while the loss tangent, is significantly higher than can be achieved for the most demanding applications, the performance is adequate, particularly in the cm wavelength range.

Domed diamond windows of 50 mm diameter can support 1 atm pressure differential at 150 μm thickness, if the diamond dome projects toward the higher pressure region.

Simulation of diamond windows is complicated by the curvature of the surface; this precludes the use of the scattering matrix formulation, and numerical methods must be used.

MS has been used to simulated thin diamond domes operating in the cm wavelength range. A commercial diamond dome grown for another application was used as a convenient source of low-cost windows. The dome dimensions are therefore not optimized to the application but represent what was available off the shelf. Because the diamond dome size was reduced to 26.4 mm OD, this window was simulated for the Ka-band frequency range. Simulations are time intensive due to the overmoded waveguide dimensions and the high relative permittivity of diamond; a high number of waveguide modes must be included in the simulation. The cell size was decreased in the region of the dielectric proportionately to the reduced wavelength. The results are shown in Fig. 12.

VI. Conclusion

The performance of broadband gyro-TWA amplifiers in the cm to mm wavelength range is dominated by stability

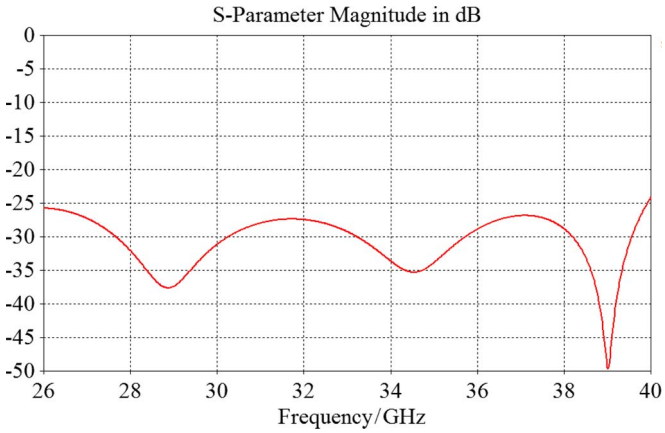

Fig. 12. Calculated return loss as a function of frequency for a 0.05 mm thick diamond window at 33-GHz center frequency.

considerations. We have shown that the control of polarization and the choice of output polarization strongly affect stability. Further work is required to improve the operational bandwidth of the linear to circular polarization converters used in amplifiers of 20% and greater bandwidth.

Gyro-TWAs using magnetic cusp electron guns are attractive in long pulse, high duty applications, and UHV amplifiers using magnetic cusp guns employing thermionic emitters have been experimentally demonstrated. Cusp electron guns can compromise the input coupler return loss if the operating band extends significantly beyond 10%, as this is often the case.

Several effective approaches to UHV broadband window design are presented. UHV compatible five-layer windows have been demonstrated in commercial standard amplifiers. Machined windows have yet to demonstrate accurate fabrication and may in any case suffer from field enhancement and breakdown. Thin dome diamond windows have been fabricated, but not yet successfully brazed due to the mismatch in thermal expansion coefficients which inevitably arises and the low resistance of the thin diamond domes to asymmetrically applied loads.

REFERENCES

[1] V. Shevchenko and A. Saveliev, "Current drive and plasma heating by electron Bernstein waves in MAST," in *Proc. AIP Conf. Proc.*, 2009, vol. 1187, pp. 457–460.

[2] J. Urban, J. Decker, Y. Peysson, P. Preinhaelter, V. Shevchenko, G. Taylor, L. Vahala, and G. Vahala, "A survey of electron Bernstein wave heating and current drive potential for spherical tokamaks," *Nucl. Fusion*, vol. 51, no. 8, p. 083050, Aug. 2011.

[3] R. S. Symons, H. R. Jory, S. J. Hegji, and P. E. Ferguson, "An Experimental Gyro-TWT," *IEEE Trans. Microw. Theory Tech.*, vol. MTT-29, no. 3, pp. 181–184, 1981.

[4] J. E. Allen and A. D. R. Phelps, "Waves and microinstabilities in plasmas-linear effects," *Rep. Progr. Phys.*, vol. 40, no. 11, pp. 1305–1368, Nov. 1977.

[5] P. E. Ferguson, G. Valier, and R. S. Symons, "Gyrotron-TWT operating characteristics," *IEEE Trans. Microw. Theory Tech.*, vol. MTT-29, no. 8, pp. 794–799, Aug. 1981.

[6] A. K. Ganguly and S. Ahn, "Self-consistent large signal theory of the Gyrotron travelling wave amplifier," *Int. J. Electron.*, vol. 53, no. 6, pp. 641–658, 1982.

[7] G. S. Park, J. J. Choi, S. Y. Park, C. M. Armstrong, A. K. Ganguly, R. H. Kyser, and R. K. Parker, "Gain broadening of two-stage gyrotron traveling wave amplifier," *Phys. Rev. Lett.*, vol. 74, no. 12, pp. 2399–2402, 1995.

[8] K. R. Chu, H. Y. Chen, C. L. Hung, T. H. Chang, L. R,. Barnett, S. H. Chen, and T. T. Yang, "Ultrahigh gain Gyrotron traveling wave amplifier," *Phys. Rev. Lett.*, vol. 81, no. 21, pp. 4760–4763, Nov. 1998.

[9] M. Garven, J. P. Calame, B. G. Danly, K. T. Nguyen, B. Levush, B. Wood, and D. E. Pershing, "A gyrotron-traveling-wave tube amplifier experiment with a ceramic loaded interaction region," *IEEE Trans. Plasma Sci.*, vol. 30, no. 3, pp. 885–893, Jun. 2002.

[10] D. E. Pershing, K. T. Nguyen, J. P. Calame, B. G. Danly, B. Levush, F. N. Wood, and M. Garven, "A TE_{11} K_a-band gyro-TWT amplifier with high-average power compatible distributed loss," *IEEE Trans. Plasma Sci.*, vol. 32, no. 3, pp. 947–956, Jun. 2004.

[11] S. J. Cooke and G. G. Denisov, "Linear theory of a wide-band gyro-TWT amplifier using spiral waveguide," *IEEE Trans. Plasma Sci.*, vol. 26, no. 3, pp. 519–530, Jun. 1998.

[12] G. G. Denisov, V. L. Bratman, A. D. R. Phelps, and S. V. Samsonov, "Gyro-TWT with a helical operating waveguide: New possibilities to enhance efficiency and frequency bandwidth," *IEEE Trans. Plasma Sci.*, vol. 26, no. 3, pp. 508–518, Jun. 1998.

[13] G. G. Denisov, V. L. Bratman, A. W. Cross, W. He, A. D. R. Phelps, K. Ronzald, S. V. Samsonov, and C. G. Whyte, "Gyrotron traveling wave amplifier with a helical interaction waveguide," *Phys. Rev. Lett.*, vol. 81, no. 25, pp. 5680–5683, Dec. 1998.

[14] G. Burt, S. V. Samsonov, K. Ronald, G. G. Denisov, A. R. Young, V. L. Bratman, A. D. R. Phelps, A. W. Cross, I. V. Konoplev, W. He, J. Thomson, and C. G. Whyte, "Dispersion of helically corrugated waveguides: Analytical, numerical, and experimental study," *Phys. Rev. E*, vol. 70, no. 4, pp. 046402-1–046402-8, 2004.

[15] W. He, A. W. Cross, A. D. R. Phelps, K. Ronald, C. G. Whyte, S. V. Samsonov, V. L. Bratman, and G. G. Denisov, "Theory and simulations of a gyrotron backward wave oscillator using a helical interaction waveguide," *Appl. Phys. Lett.*, vol. 89, no. 9, pp. 091504-1–091504-3, 2006.

[16] S. V. Samsonov, A. D. R. Phelps, V. L. Bratman, G. Burt, G. G. Denisov, A. W. Cross, K. Ronald, W. He, and H. Yin, "Compression of frequency-modulated pulses using helically corrugated waveguides and its potential for generating multigigawatt RF radiation," *Phys. Rev. Lett.*, vol. 92, no. 11, pp. 118301-1–118301-4, Mar. 2004.

[17] W. He, C. G. Whyte, E. G. Rafferty, A. W. Cross, A. D. R. Phelps, K. Ronald, A. R. Young, C,. W. Robertson, D. C. Speirs, and D. H. Rowlands, "Axis-encircling electron beam generation using a smooth magnetic cusp for gyrodevices," *Appl. Phys. Lett.*, vol. 93, no. 12, pp. 121501-1–121501-3, Sep. 2008.

[18] C. R. Donaldson, W. He, A. W. Cross, A. D. R. Phelps, F. Li, K. Ronald, C. W. Robertson, C. G. Whyte, A. R. Young, L. Zhang, P. McElhinny, A. D. R. Phelps, and K. Ronald, "Design and numerical optimization of a cusp-gun-based electron beam for millimeter-wave gyro-devices," *IEEE Trans. Plasma Sci.*, vol. 37, no. 11, pp. 2153–2157, Nov. 2009.

[19] T. Gray, D. N. Smithe, and L. D. Ludeking, Mission Research Corporation.

[20] M. Thumm, "Progress on Gyrotrons for ITER and future thermonuclear fusion reactors," *IEEE Trans. Plasma Sci.*, vol. 39, pt. 1, no. 4, pp. 971–979, 2011.

C. G. Whyte, photograph and biography not available at the time of publication.

K. Ronald, photograph and biography not available at the time of publication.

A. R. Young, photograph and biography not available at the time of publication.

W. He, photograph and biography not available at the time of publication.

C. W. Robertson, photograph and biography not available at the time of publication.

D. H. Rowlands, photograph and biography not available at the time of publication.

A. W. Cross, photograph and biography not available at the time of publication.